Thermoelectric harvesters and the internet of things: technological and economic drivers

JPhys Energy

PAPER

Thermoelectric harvesters and the internet of things: technological and economic drivers

Dario Narducci

University of Milano Bicocca, Dept. Materials Science, v. R. Cozzi 55, I-20125 Milan, Italy

E-mail: dario.narducci@unimib.it

Keywords: thermoelectricity, wireless sensing networks, internet of things, batteries, power costs

OPEN ACCESS

RECEIVED
31 December 2018

REVISED
18 February 2019

ACCEPTED FOR PUBLICATION
4 March 2019

PUBLISHED
17 April 2019

Abstract

The spectacular growth of networks of intercommunicating sensing nodes has generated a request for alternate, renewable power sources. Thermoelectric generators (TEGs), either conventional or integrated, are possible candidates. This paper analyzes the usability of TEGs as alternate power sources for wireless sensor network. It is shown how TEGs meet power requirements of low-power sensing nodes and how they outperform batteries as of the installation costs. Factors still hampering TEG wider use are also reviewed and commented upon, and an outlook at specific applications where TEGs might be rapidly deployed is provided.

1. Introduction

In 2006 devices autonomously exchanging information were reported to have outnumbered humans connected to Internet worldwide [1]. Communication among devices has served the aim of enabling cooperative behaviors and reactions to external stimuli or events, from evaluation of alerts to concerted actions following changes of environmental conditions. Connected devices may be simple sensing nodes (SNs) in a network or may be sensing and actuating elements of complex nets, and are being more and more deployed in the most diverse fields, from medical diagnostics to security, from predictive maintenance to environmental safety—not to forget their use for energy saving in buildings.

In most situations, devices are remotely deployed, so that maintenance may be either inconvenient or impossible. Therefore, a need raises for nodes that not only exchange data wirelessly but also, often, operate maintenance-free over their whole predicted lifetime. From the powering viewpoint this implies that either they have to embed energy sources consistent with their operative lifespan or that, if working off-grid, renewable energy converters must sit on board. Among renewable converters, thermoelectric generators (TEGs) may play a relevant role, whenever temperature differences are available at deployment sites.

TEGs are devices capable to partially convert heat fluxes into electric power with no moving parts. TEGs are well known to be highly reliable, with lifetimes often largely exceeding those of the devices they power [2]. As such, TEGs have found extended applications in mission-critical contexts (e.g. as power sources in outer space probes). However, especially over small temperature differences their efficiency is quite small, and this has discouraged their use till now for macroharvesing (i.e. to generate electric power above kilowatts), where traditional heat engines are still largely preferred. However, for distributed applications as those required to enable communication within wireless sensing networks (WSNs) and, in more general terms, for many novel contexts arising with the development of the so-called Internet of things (IoT), the electric power outputs they can achieve may be suitable to replace or at least to supplement ordinary power storage devices (batteries).

Aim of this paper is to analyze contexts and archetypical applications where TEGs may compete with batteries as power supplies. This involves three levels of analysis:

(i) energy requirements, namely a comparison between the capabilities of energy storage of batteries versus the energy demand of services SNs;

Table 1. Power consumptions for commercial data transmission protocols. Data from [7]. Energy per connection computed for an exemplar communication event of 1.8 s receive and 20 ms transmit times (1% active state) [6].

Protocol	Sleep (mW)	Receive (mW)	Transmit (mW)	Energy per connection (mJ)
WiFi	0.01	90	350	169
Zigbee	0.004	84	72	153
Bluetooth	0.008	28.5	26.5	52

(ii) power requirements, namely (a) a comparison between the electric power that a TEG can generate and the power demand of SNs; and (b) the capabilities of TEGs and batteries to timely respond to surge of power needs by the devices they power; and

(iii) economic competitiveness, namely a comparison between power and energy costs of TEGs and batteries.

Such an analysis will encompass both standard TEGs, already available on the market; and microTEGs, i.e. planar TEGs, currently being prototyped, that may be integrated on microelectronic boards.

This paper is organized as follows. In section 2, the power and energy requirements of typical SNs will be reviewed and commented upon, to set a reference for the comparative analysis of energy and power availability out of TEGs and batteries (sections 3 and 4). Cost analyses will be the subject of section 5. Comparisons of electric sources will be discussed in section 6, while conclusions concerning the profitability of thermoelectric technologies in WSNs and in the IoT will be reached in section 7, also discussing issues related to the geo-availability of raw materials needed by both technologies.

2. Power and energy requirements of SNs

In general terms, SNs share with conventional sensors their capabilities (a) to measure one or more quantities (chemical, physical, electrical, environmental, etc.) and (b) to convert such a measurement into an electric signal. However, SNs further (c) store information temporarily, (d) elaborate it, and then finally (e) transmit data to some remote logging/processing station and/or to other nodes in the network.

With a few exceptions (mostly related to some self-heated chemical sensors [3]) and despite often sophisticated local computational capabilities, the most power-demanding SN operational step is data transmission [4]. This enables large classes of widely differentiated devices to be analyzed along.

While SN power consumption in sleep mode is relatively small (typically in the order of 10 μW or less [5, 6]), during the duty cycle power requirements surge to $\approx$1 mW over a time span of about 2 s (listening and transmit times). Frequency of data transmission largely varies. While event-driven transmission is customary only in alarm sensor networks, in most cases data exchange is time-driven, occurring from every minute to every some hours. This largely reduces the average power requirements of the SN [6].

Table 1 summarizes typical power requirements in different working states along with exemplar energy consumptions per connection for SNs operating using commercial data transmission protocols. Since transmission events may occur with widely different frequencies, power sources are requested to provide average powers ranging from some tens of microwatts (Bluetooth connection occurring every hour) to a few tenth of watts (WiFi connection occurring every second). Thus, energy and average power requirements are to be assumed to span more than four orders of magnitude. It should be stressed that any attempt to more exactly quantify average power requirements of SNs is pointless, since they intrinsically depend on their operational mode and on their context of use.

An additional feature more and more often met in SNs is their capability of locally processing information. Processors, either single-core or multi-core microcontroller units (MCUs), are embedded in the SN. As anticipated, the engineering effort has led to develop ultra-low power processors, with power consumptions down to 15 mW (in their active state). Furthermore, MCUs spend most of their time in sleep mode, so that, unless the application requires a high computational workload, average power requirements remains negligible compared to radio transmission [4].

Typical commercial sensor nodes characteristics and average power consumption along with currently used portable power supplies are reported in table 2.

Table 2. Characteristics of commercial sensor nodes and typical contexts of use. Powers shown in the table refer to power requirements when the device is in its active mode. Data from [8].

Id	Range (m)	Components	Power supply	Device area (cm^2)	Application
WeC	4.6	MCU, Storage, light and temp. sensors	Coin cell, 24 mW	6.25	Environmental sensing
Rene 2000	30.5	MCU, Storage, GPIO, SI	Battery 24 mW	n.a.	Environmental analyses
Mica	61	MCU, Storage, GPIO, SPI	2 × AA 27 mW	17.36	Environmental, bridge stability, preventive maintenance
Mica2Dot	152	MCU, Storage, GPIO, SPI	2 × AA 44 mW	7.75	Environmental, home net, military
Imote 2	91.5	MCU, Camera, Storage, SI	3 × AA 86.8 mW	16.92	Image processing, industrial monitoring, vibration analysis

Note. SI: sensor interface; GPIO: General Purpose Input Output; SPI: Serial Peripheral Interface; n.a.: not available.

3. Energy and power capabilities of TEGs

As for any heat engine, TEG power output scale with its conversion efficiency η_{TEG} and the heat flux (in W m^{-2}). Conversion efficiency depends in turn on the materials property through the materials thermoelectric figure of merit $zT = \sigma\alpha^2 T/\kappa$ (where σ is the electrical conductivity, α is the Seebeck coefficient, κ is the thermal conductivity, and T is the absolute temperature) and with the temperature of the hot and cold sink the device exchange heat with [9].

In typical applications, TEGs are made of thermoelectric elements (named *legs*) of *p* and *n*-types connected in an electrical series while forming a parallel thermal circuit with the heat sinks. The device figure of merit ZT reads:

$$ZT = \frac{(|\alpha_p| + |\alpha_n|)^2}{(\sqrt{\kappa_p/\sigma_p} + \sqrt{\kappa_n/\sigma_n})^2} T, \tag{1}$$

where subscripts *p* and *n* label transport coefficients of the *p* and *n*-type legs. The device efficiency may then be written as [9]

$$\eta_{TEG} = \frac{T_H - T_C}{T_H} \frac{\sqrt{1 + Z\bar{T}} - 1}{\sqrt{1 + Z\bar{T}} + T_C/T_H}, \tag{2}$$

where subscripts C and H refers to the cold and the hot sink, respectively, while $\bar{T} = (T_H + T_C)/2$. Equation (2) reports the largest conversion efficiency for a device operating over a temperature difference small enough to neglect the temperature dependence of the transport coefficients (constant-property limit—CPL). While CPL is surely inappropriate in a number of relevant applications, it is a more than reasonable approximation for microTEGs and, more in general, for devices converting heat over temperature differences not exceeding a few tens of degrees. Also, as further discussed in the next subsection, efficiency predicted by equation (2) neglects thermal contact resistances, which scale down the effective temperature difference applied to the thermoelectric legs. Therefore, it is to be considered as an upper efficiency limit. with real efficiencies being unavoidably lower.

3.1. Standard TEGs

As just mentioned, in standard TEGs the achievable efficiencies are often dumped by several factors. First, thermal contact resistances and thermal resistances originating from TEG packaging decrease the effective temperature difference sensed by the device. Second, thermal cross-talk among TEG legs partially dissipate the heat flowing trough the device, making it unavailable for conversion. Finally, the generated electric power may be back-converted into heat by parasitic (contact) electrical resistances and by DC–DC converters often needed to bring TEG output voltages into the volt range.

Despite these limitations, over the last decade major improvements have been achieved in TEGs. Novel materials (or improved standard materials) have been reported having ZT values well in excess of 2 [10]. However, none of them has been yet qualified for production, and all of them reach anyway high ZT only at high temperatures. More practically relevant advances have been achieved on TEG design, which has undergone

Table 3. Reported specifications of selected commercial TEGs.

Maker and model	Footprint (cm^2)	Max T (°C)	Electric power output (W)	Input heat flow (W)	Thermal resistance ($K\ W^{-1}$)
European Thermodynamics					
MGM250-49-10-12HS	1.8 × 1.8	250	1.33	23	
GM250-49-45-25	6.2 × 6.2	250	15.24	312	
GM250-127-28-12	6.2 × 6.2	250	25.5	510	
Hi-Z					
HZ-2	2.9 × 2.9	250	2.25	50	
HZ-9	6.3 × 6.3	250	9.0	185	
HZ-14	2.9 × 2.9	250	14.0	350	
HZ-20	7.5 × 7.5	250	20.0	475	
Kryotherm					
TGM-127-1,0-0,8	3 × 3	200	5.1		1.69
TGM-127-2,0-1,3	4.8 × 4.8	250	12.6		0.69
Mars-35	26.0 × 9.2	500	35	565[a]	
Mars-65	26.0 × 9.2	500	65	878[a]	
Marlow (II-VI Inc.)					
TG12-2.5-01LS	3.4 × 3.0	230	2.71		3.33
TG12-4-01LS	3.4 × 3.0	230	4.05		2.21
TG12-6-01L	4.5 × 4.0	230	6.16		1.47
TG12-8-01LS	4.5 × 4.0	230	7.95		1.13
Micropelt GmbH					
TGP-651	1.5 × 1.0	85	0.009		28
TECTEG					
TEG1-4199-5.3	4.0 × 4.0	300	7.5	152	
TEG1-12611-6.0	5.6 × 5.6	300	14.6	365	
TEG1-PB-12611-6.0	5.6 × 5.6	350	21.7	310	
TEGpro					
TGPR-10W-4V-40S	4.0 × 4.0	330	10	188	
TGPR-22W-7V-56S	5.6 × 5.6	330	21.7	415	

[a] Estimated.

significant enhancements related to a more accurate control of the thermal chain within the device and in the whole thermal circuit the device sits in. Suppression (or at least a severe reduction) of the thermal cross-talk among legs has enabled the fabrication of TEGs with optimized geometry. A reduced filling factor (defined as the ratio between the total leg cross-sectional area and the TEG footprint) enhances TEG efficiency by increasing the temperature drop across legs. At the same time, since smaller filling factors imply the use of smaller quantities of thermoelectric materials, this has also made economically viable the development of TEGs with larger exchange areas. When operating over fixed heat fluxes (Neumann boundary conditions), this enables larger temperature difference to develop, increasing conversion efficiency [11]. Along the same directions, use of heat pipes and the enhanced capabilities of heat dissipaters at the TEG cold side has led to harvesters capable of power outputs in the order of watts over temperature differences of 50 K [12].

Table 3 summarizes reported electric power outputs and footprint areas of commercial, off-the-shelf TEGs. Power densities may be as high as 0.7 W cm^{-2} for $T_H = 350$ °C.

3.2. Integrated TEGs

Integrated TEGs (microTEGs) are currently still under development, and have found only very limited deployment. They adopt two types of layouts: (1) parallel layouts, where heat flow is parallel to the substrate and thermoelectric legs are suspended or anyway thermally insulated from the substrate (figure 1); (2) normal layouts, where heat flow is normal to the substrate but cavities are created underneath the thermoelectric legs so to prevent major thermal shunts from the substrate (figure 2). Both layouts have advantages and shortcomings. The parallel layout, while ideally compatible with the microelectronic (planar) technology, may be either limited by the thermal shunt due to the membrane the legs sit on and by the mechanical stability (fragility) of fully suspended thin films, nanolayers or nanowires. Normal layouts are more robust but largely underuse the temperature difference between hot and cold heat sinks. Over the last years interesting examples of smart solutions to both issues have been reported in the literature. Use of bulk silicon frameworks with Si nanowires grown across facing sides of the framework were reported [13, 14], largely overcoming the issue of fragility; and normal layouts with thinned substrates minimizing series thermal resistance were demonstrated [15]. In both

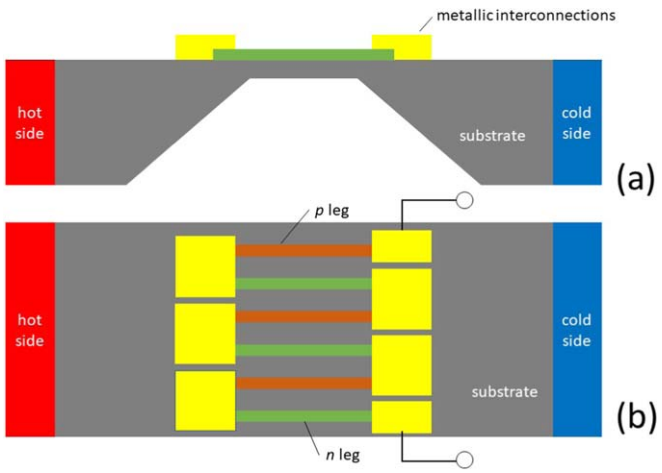

Figure 1. (a) Cross- and (b) top-views of the parallel layout of microTEGs. Heat is injected parallel to the substrate and is forced to flow mostly through the thermoelectric legs. When the device operates between two thermostats, the large thermal resistance of the legs causes most of the temperature difference between hot and cold sinks to fall over the legs, maximizing the efficiency.

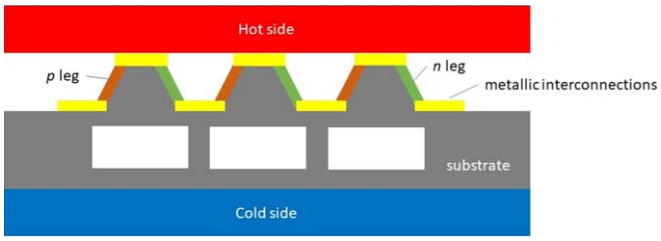

Figure 2. Schematics of the normal layout for microTEGs. Heat sinks face the substrate, with heat flowing normal to it. Since the height of the thermoelectric legs is micrometric, and therefore their thermal resistance is small, cavities are generated within the substrate underneath the legs to limit thermal shunts by the substrate.

cases, microTEGs operate converting relatively large heat fluxes (due to the small thermal areal resistance of micrometric-sized legs) into electric power over small temperature differences, since the proximity of the two heat sinks disables the establishment of temperature differences comparable to those used in standard TEGs.

Both layouts have enabled improved performances over the last twenty years, moving from 1.5 μW (parallel layout, over a temperature difference of 10 K) [16] and 1.3 μW cm^{-2} (normal layout, over a temperature difference of 5 K) [17] to the recently achieved power density of 12.3 μW cm^{-2} (normal layout, over a temperature difference of 31 K) [18].

4. Energy and power capabilities of batteries

Batteries are the most natural option to supply electric power to off-grid devices. They are commercially available and technologically reliable. Although a large number of different battery types are available, at present only alkaline, nickel metal-hydride and lithium-ion batteries are used to power portable devices.

Disposable alkaline batteries are primary batteries making use of the electrochemical reaction between metallic Zn and MnO_2, using KOH as electrolyte [19]. Rechargeable alkaline batteries are instead secondary batteries. Their structure is similar to that of disposable alkaline cells, with a cathodic paste of MnO_2 pressed into a steel can, forming the positive electrode, and the negative electrode consisting of zinc powders suspended in a gel. Rechargeable alkaline batteries differ from disposable ones as they also include additives (e.g. $BaSO_4$) in the cathode, which improve cycling and increase performances by preventing the formation of insoluble manganese compounds. Also, ZnO is added to the cathodic paste to reduce generation of H_2. Alkaline batteries have a higher energy density and longer shelf-life than Zn-carbon cells, and still account for 80% of manufactured batteries in the US [20].

Nickel Metal-Hydride batteries (NiMH) are rechargeable batteries based on the electrochemical reaction between NiO(OH) and a metal, using KOH as the electrolyte [21]. NiMH batteries have energy densities close to those of a lithium-ion battery. The metal in the negative electrode is usually an intermetallic compound of

Table 4. Specific energy and power of the most common classes of rechargeable batteries along with typical ranges of durability (cycles of recharge) and energy costs. Data from [26] and [27].

Battery type	Specific energy		Specific power	Durability	Energy cost
	($J\ g^{-1}$)	($J\ cm^{-3}$)	($W\ g^{-1}$)	(cycles)	(USD/MJ)
Lead Acid	119–151	216–396	0.18	500–800	28–56
NiCd	144–216	180–540	0.15	2000	83–170
NiMH	216–432	504–1080	0.25–1.0	500–2000	83–170
NiZn	360	1008	>3.0	400–1000	93–138
$LiCoO_2$	360–954	900–2232	0.25–0.340	400–1200	83–280
$LiFePO_4$	324–396	792	≈2.4	2000	83–280

formula ReM_5, where Re is a rare-earth mixture of La, Ce, Nd, and Pr; and M is Ni, Co, Mn, or Al. Higher-capacity negative electrode materials are also available, based on alloys of Ti or V with Zr or Ni and containing small amounts of Cr, Co, Fe, or Mn. Any of these alloys reversibly form a mixture of metal hydrides. Hydrogen evolution is suppressed, and the charging energy is converted to heat on overcharging. This allows NiMH batteries to be sealed and maintenance-free [21].

Lithium-ion batteries are also rechargeable batteries, making use of an intercalated lithium compound as one electrode material. They are very commonly used for portable electronics due to their high energy density, minor memory effect and low self-discharge. Chemistry may quite vary. Lithium-ion batteries used in portable electronics mostly use cells based on $LiCoO_2$. They provide high energy density but may incur in safety risks, especially when punctured [22]. Alternate chemistry is provided by $LiFePO_4$, $LiMn_2O_4$, Li_2MnO_3, and $LiNiMnCoO_2$ cells, where the lower energy density is compensated by longer lifetimes and lower safety risks. Such second types of batteries are used for electric tools and medical equipment, and are being considered for automotive applications. Experimental lithium–sulfur batteries promise even higher energy densities.

In lithium-ion batteries, both electrodes allow lithium ions to move in and out through intercalation and deintercalation. During discharge, Li^+ ions move from the anode, usually made of graphite, to the cathode. Therefore, the cathodic half-reaction leads to Li^+ intercalation (e.g. $CoO_2 + Li^+ + e^- \rightarrow LiCoO_2$) while the anodic half-reaction deintercalates lithium, oxidizing it from metallic to ionic [23]. The resulting cell voltage is too large to use aqueous electrolytes. Therefore, either lithium salts (e.g. $LiPF_6$, $LiBF_4$ or $LiClO_4$) dissolved in an organic solvent or ionic liquids are used [24]. Recently, solid electrolytes, either glassy or ceramic, have also been considered. Among the latters, lithium superionic conductors (LISICON) and perovskites have surfaced as the most promising candidates [25].

Table 4 summarizes specific energy andc power of several classes of batteries.

5. Energy and power costs

5.1. Battery cost structure

Energy costs for rechargeable commercial batteries are displayed in table 4. It should be noted that such costs also include disposal (end-of-life) costs.

5.2. TEG cost structure

TEGs are partially industrialized devices. Therefore, no stabilized power cost is available yet. Therefore, TEG cost structure will be analyzed using cost models, and then compared to current TEG *prices* when available.

5.2.1. Standard TEGs

We make use of the analysis of the cost structure for conventional (non-integrated) TEGs developed by Yee *et al* [11]. Capital costs were evaluated by considering volumetric module costs χ'''_{TEG} (USD/m^3), i.e. costs of TEG components scaling with the TEG volume, areal module costs χ''_{TEG} (USD/m^2), scaling with the TEG contact area, and heat exchangers costs β_{HX} ($USD/(W\ K^{-1})$). Therefore, total TEG cost χ_{TEG} (in USD) accounts to

$$\chi_{TEG} = (\chi'''_{TEG} L + \chi''_{TEG}) A_{TEG} F + \beta_{HX} U A_{TEG}, \tag{3}$$

where F is the filling factor, A_{TEG} is the total heat exchange area (TEG footprint), L is the leg length, and U is the heat transfer coefficient. The power output per unit area p_{TEG} reads [11]

$$p_{TEG} = \frac{\alpha_{pn}^2 \sigma F \Delta T^2}{4} \times \frac{L/4}{(2(\kappa F/U) + L)^2}, \tag{4}$$

Table 5. Parameters used in the evaluation of power costs of conventional TEGs. Materials costs refer to Bi_2Te_3. Data from [11, 29].

Cost parameters	Value	Units
χ'''_{TEG}	0.89	USD/cm^3
χ''_{TEG}	0.017	USD/cm^2
β_{HX}	18.00	USD/(W K^{-1})

where κ and σ are the thermal and electric conductivity of the leg elements (assumed to be the same for the p and n elements) and $\alpha_{p-n} \equiv \alpha_p - \alpha_n$. Therefore, equations (3) and (4) immediately return the cost per unit power (in USD/W)

$$c_{TEG}(L, F) = \frac{16}{\alpha_{p-n}^2 \sigma \Delta T^2}\left(2\frac{\kappa F}{UL} + 1\right)^2\left(\chi'''_{TEG}L^2 + \chi''_{TEG}L + \frac{\beta_{HX}UL}{F}\right). \quad (5)$$

Equation (5) admits no global minimum on F and UL/κ. Nonetheless, the $c_{TEG}(L, F)$ surface displays a narrow region around the line $F = UL/(2\kappa)$ where c_{TEG} takes low values, resulting from a competition between costs and thermoelectric performances [11]. For smaller L (at constant F) materials, costs decrease along with the temperature drop across the device, so that also power output decreases. Furthermore, a characteristic point exists below which any further decrease of L and F has only marginal benefits on c_{TEG}.

Exemplar values for χ''_{TEG}, χ'''_{TEG}, and β_{HX} (table 5) predict device costs for Bi_2Te_3–based TEGs in acceptable agreement with market *prices*. As an example, for Marlow TEG mod. TG12-8-01LS (table 3) the model predict a cost of 5.63 USD while bulk price is around 25 USD [28]. The apparently large difference between price and estimated cost finds a justification considering the major price markup expected for a small volume production. Applying the model to Bi_2Te_3 (currently the material dominating TEG technology), one obtains an optimized power cost c_{TEG} of 38.5 USD/W, which also includes the cost arising from the heat exchanger (currently about 30% of the total cost) [29].

5.2.2. Micro-TEGs

To the best of our knowledge, no attempt has been made yet to estimate power costs for integrated TEGs. Evaluations of manufacturing costs for integrated devices is reportedly complicated by a number of factors that may enter the production process upon prototyping, making preliminary estimates largely overoptimistic. In addition, for non-standard applications such as integrated TEGs many parameters commonly used in microelectronics might show inadequate. Furthermore, not easier is the computation of the power output achievable with planar thermoelectric devices, due to the significant shunts often occurring and the very limited temperature differences that may be applied across TEG legs. This notwithstanding, preliminary and unavoidably crude computations of power costs are believed to be of interest when considering the use of thermal harvesters for IoT.

A recent review of microthermoelectric generators [30] showed how almost all microTEGs analyzed, modeled, and prototyped over the last ten years had made use of standard microelectronic technologies. Therefore, we will limit the current analysis to generators obtained through standard planar manufacturing processes, although alternate approaches have been reported [31] and could provide viable routes of fabrication over the next future.

Cost of fabrication (not to be confused with the cost of ownership) for IC devices is basically set by three factors, namely the number of required lithographic steps, the yield of the process, and the testing cost. Furthermore, cost per device depends on the number of dies per processed wafer. Materials costs, instead, have a negligible impact on final TEG costs.

Cost per lithographic step, which depends on mask costs further than to exposure and resist costs, dramatically scales down with the number of processed wafers. A reasonable cost model for microTEGs may be inherited from micro-electromechanical systems (MEMSs), which share with microTEGs small volumes of production and a relative manufacturing simplicity (compared to CPUs and DRAMs). In general terms, microTEGs require $\leqslant$5 masking steps. Costs per wafer (12 inches) are computed to range between 365 USD (single lithographic step—1L) to 620 USD (five lithographic steps—5L) [32]. For 20 $\times$ 20 mm^2 square dies, 140 microTEGs per wafer are obtained, at a cost ranging from 2.61 to 4.43 USD/die. Such costs sum to packaging costs of about 1.50 USD/die [33], totaling to a cost ranging from 1.03 to 1.48 USD cm^{-2}. In view of the output power densities (cf section 3.2), this leads to a grossly estimated power cost ranging between 60 USD/W (1L design) and 120 USD/W (5L design).

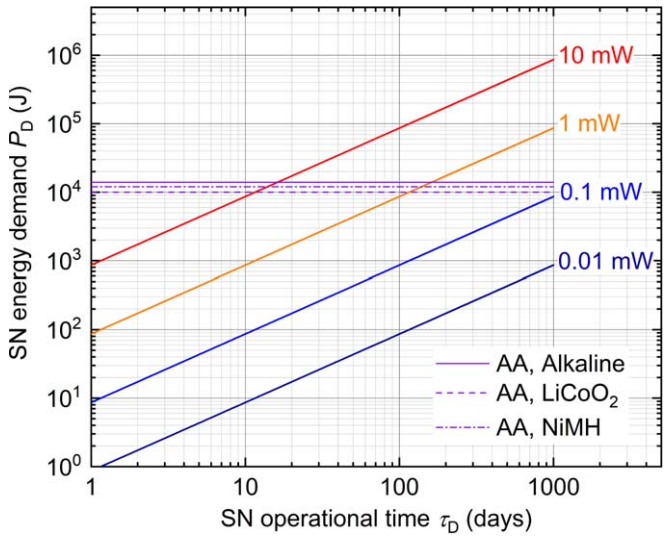

Figure 3. Energy demand by typical SNs versus time of use compared to energy available to various types of batteries. Crossing points between energy lines and stored energies report expected maintenance (replacement and recharging) times. Note that the graph refers to SNs powered by a single AA battery. Use of two or more batteries slightly extends operational times.

Power cost for integrated TEGs may look discouraging, compared to standard TEGs. However, two points are to be considered. First, it is simple to verify that, differently from standard TEGs, the cost structure of integrated TEGs is basically independent of dissipater costs. Even for β_{HX} larger by a factor one hundred compared to standard macroscopic heat dissipaters, dissipater contribution to the final power cost remains negligible. Stated differently, the cost of integrated TEGs is not bound by the cost of a collateral technology. Second, the cost model used in this estimate is that of MEMSs. For larger volumes of production (as those required by IoT), production costs might largely scale down, as usual for integrated electronic devices.

6. Comparison between batteries and TEGs

As anticipated, batteries and TEGs may be now compared both in view of energy and power requirements of off-grid devices and of the cost structures of the two power sources.

Figure 3 displays energy demand E_D of devices with exemplar *average* power consumptions P_D between 10 and 0.01 mW as a function of their operational time τ_D—overlaid with energy capabilities E_b of some common classes of batteries. Crossing points return battery replacement times τ_r. Since power requirements are easily met by any type of battery, they are not commented upon. The plot shows that for average power demand $\leqslant$0.1 mW, conventional batteries are capable of powering the SNs for times longer than 3 years, which can be taken as the time of technological obsolescence (and possibly also as the lifetime) of the SNs. Therefore, no maintenance is needed. Instead, for larger average power demands, batteries need to be replaced (recharged) with a periodicity ranging from 10 to 100 d.

For conventional TEGs, the relevant plot is that reporting electric power output achievable by TEGs P_{TEG} as a function of the heat exchange area A_{TEG}—overlaid with the power requirements of SNs (figure 4). Due to the very long lifetime of TEGs (>20 years) [2], energy constraints are not significant in this case, and are not considered. In this plot, crossing points set the minimal exchange areas of the TEG. For conventional TEGs, power outputs are capable of satisfying the average power requirements of any SN even when exchanging heat over areas $\leqslant$0.1 cm^2. For footprint areas comparable to those of the SNs, power availability exceeds the SN demand by about two orders of magnitude, therefore largely mitigating losses of performance due to suboptimal thermal chains. For integrated TEGs, instead, only SNs with average power demand $\leqslant$0.1 mW may be effectively serviced.

It may be worth remarking that available heat fluxes and temperature differences may largely vary depending on the TEG deployment scenario. Although macroTEGs may operate over large temperature differences ($\leqslant$200 K), leading to power outputs of $\approx$0.1 W cm^{-2}, outputs may appreciably scale down when smaller temperature differences and/or smaller heat inputs are available. Therefore, estimates of power output densities need to be actualized to the specific context of use [34].

The two plots well summarize the issues setting technological and economic viability of the two approaches. Manifestly enough, neither batteries nor TEGs may be ruled out as powering solutions. Instead, needs of

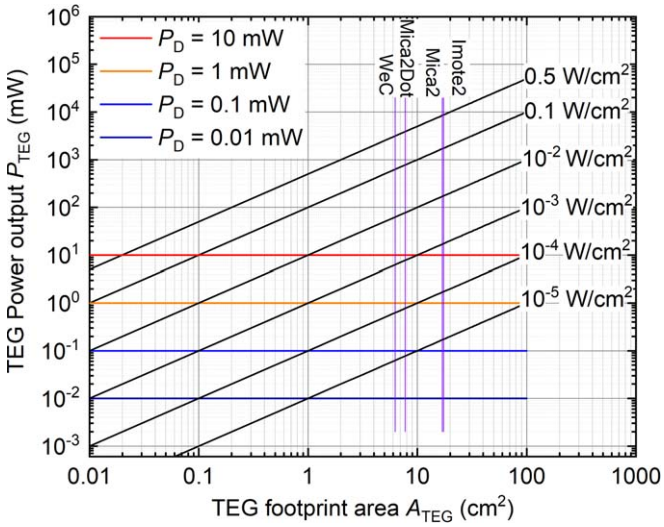

Figure 4. TEG power outputs versus TEG footprint (heat exchange) areas compared to average power demand of typical SNs. For comparison, vertical lines display the footprint areas of some common SNs (see table 2).

replacements (and therefore of servicing) for battery-powered SNs set the *operational* (maintenance) costs of this more conventional solution; while TEG area sets the *capital* (installation) costs of thermal harvesters. This is one of the main results of this analysis. Choice of either solution meet stringent technological constraints only for integrated TEGs, forcing them to be discarded *a priori* for power-hungry SNs. In all other cases, selection should be driven by economic considerations, accounting for the onset of all costs (installation and maintenance) underlying them.

Installation costs follow immediately from previously reported data. However, metrics are different for batteries and TEGs, as they are in USD/J (C_b) for the formers and in USD/W (c_{TEG}) for the latters. Thus, the comparison must be carried out considering the lifetime of the SN. This also enables to account for the maintenance (battery replacement) costs (χ_m, USD/event).

The energy needed by a SN over its lifetime τ_D is $E_D = P_D \tau_D$. If a battery is chosen, the installation cost is then $C_b E_D$ while for a TEG the installation cost accounts to $c_{TEG} P_D$. Furthermore, replacement costs for batteries are $\chi_m \frac{P_D \tau_D}{E_b}$ (where E_b is the electric energy stored in the battery). Therefore, powering cost χ_D for the SN (in USD) reads

$$\chi_D = \begin{cases} P_D \tau_D \left(C_b + \dfrac{\chi_m}{E_b} \right) & \text{(batteries)} \\ c_{TEG} P_D & \text{(TEGs)} \end{cases}. \tag{6}$$

Maintenance costs are strongly dependent upon the context of WSN deployment (remoteness of the SNs and width of the area covered by the WSN) and by the local labor cost. For labor cost ranging from 5.6 USD/h (China) to 22.95 USD/h (USA) [35] and for single maintenance events requiring from 10min to 2 hours, χ_m spans from 1 to 46 USD/event.

Figure 5 shows the total powering cost χ_D of a SN as a function of χ_m for batteries and TEGs (both standard and integrated) supplying power to SNs with average power demands from 0.01 to 10 mW. It is immediate to realize that TEGs provide a far more economic way to power SNs. This is a possibly obvious result, yet somewhat undervalued. For a SN requiring an average power of 1 mW and with a lifetime of 1000 d, the total energy that must be supplied accounts to 6.24×10^5 J. At an energy cost of 150 USD/MJ (table 4) this implies a powering cost with batteries of 9.36 USD (neglecting maintenance) while for TEGs the cost could range between 0.04 and 0.12 USD, were generators with minimal footprint area available. This major difference simply reflects the fact that waste heat is free while batteries need to be charged.

7. Discussion and conclusions

The results of the technological and economic analyses reported in the previous sections hardly explains the yet marginal use of TEGs in WSNs and IoT. Beyond the inertia to deploy novel technologies replacing standard ones, some non-economical and non-technological factors must be considered that currently hamper a larger utilization of thermal harvesters.

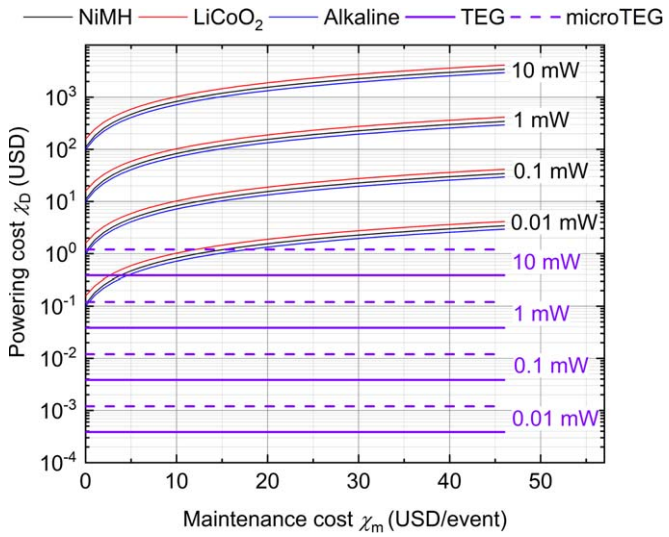

Figure 5. Powering cost χ_D using batteries or Bi_2Te_3-based TEGs as a function of the maintenance cost per event χ_m for typical average power demand of the SNs.

First, while batteries requires no modification of SN design, this is not the case for TEGs. The overall SN must be conceived in such a way to optimize heat intake (hot side) and dissipation (cold side), making the overall system more complex to devise. Also, deployment requires additional care (and expertise), raising the risk of installation failure.

Second, for large the cost saving may be, it often marginally impacts the overall cost of the WSN, which is set by electronics (capital cost) and surveillance (maintenance costs). Thus, the economic driver in itself, although substantial from the energetic viewpoint, may turn out to be negligible in more general terms.

Third, TEG requires additional power-conditioning electronics to be integrated with the harvesters. Maximum power point trackers and (super)capacitors or buffer rechargeable batteries are needed for TEG startup and to meet power surges occurring when SNs enter their active state (for communication and/or data processing). Although additional costs are nowadays small enough not to significantly change the economic comparison reported in section 6 [36–38], encompassing them in the design of SNs are believed to slow down consideration of TEGs as alternate power supplies.

Finally, TEGs are mostly available as standard, off-the-shelf devices. Therefore, power costs are normally larger than needed, since the TEG footprint area cannot be optimized for a specific SN power and energy demand.

Nevertheless, the analysis presented in this paper clearly shows that thermoelectric harvesters have the full technological momentum to compete with more conventional portable power sources for IoT; and that cost factors are *not* the hurdle limiting their wider use. Implementation-related hurdles might be overcome, letting TEGs enter the IoT market, wherever battery replacement would be simply unfeasible, making alternate choices unavailable. Embedded sensors to monitor the stability of bridges and buildings are among the possible examples. In such a context, temperature differences between 10 and 20 K arise between asphalt concrete and the pavement subgrade [39] that sustains power output densities of $\approx 10^{-3}$ W cm^{-2}, sufficient to power most SNs already for TEG footprints of $\approx$10 cm^2 (see figure 4).

In conclusion, one may expect that the development of WSNs over the next years might provide thermoelectric research and development with the long-awaited opportunity to emerge as a fully recognized tool not only to recover wasted heat but also to locally convert it into the critical, high-value low power needed to support specific applications in the IoT.

ORCID iDs

Dario Narducci https://orcid.org/0000-0002-3307-1070

References

[1] Mukhopadhyay S C and Suryadevara N K 2014 Internet of things: challenges and opportunities *Internet of Things: Challenges and Opportunities* ed S C Mukhopadhyay (Berlin: Springer) pp 1–17
[2] Yang J and Caillat T 2006 Thermoelectric materials for space and automotive power generation *MRS Bull.* **31** 224–9

[3] Fàbrega C, Casals O, Hernández-Ramírez F and Prades J D 2018 A review on efficient self-heating in nanowire sensors: prospects for very-low power devices *Sensors Actuators* B **256** 811
[4] Rossi D, Loi I, Pullini A and Benini L 2017 Ultra-low-power digital architectures for the internet of things *Enabling the Internet of Things: From Integrated Circuits to Integrated Systems* ed M Alioto (Berlin: Springer) pp 69–93
[5] Raghunathan V, Schurgers C, Park S and Srivastava M B 2002 Energy-aware wireless microsensor networks *IEEE Signal Process. Mag.* **19** 40–50
[6] Knight C, Davidson J and Behrens S 2008 Energy options for wireless sensor nodes *Sensors* **8** 8037–66
[7] Choperena M 2013 RFID-powered sensors can play a big role in the internet of things *RFID J.* **11** 62
[8] Akyildiz I F, Su W, Sankarasubramaniam Y and Cayirci E 2002 Wireless sensor networks: a survey *Comput. Netw.* **38** 393–422
[9] Narducci D, Bermel P, Lorenzi B, Wang N and Yazawa K 2018 A primer on thermoelectric generators *Hybrid and Fully Thermoelectric Solar Harvesting* (*Springer Series in Materials Science* vol 268) (Berlin: Springer) ch 2 pp 11–43
[10] Beretta D *et al* 2018 Thermoelectrics: from history, a window to the future *Mater. Sci. Eng.* R accepted (https://doi.org/10.1016/j.mser.2018.09.001)
[11] Yee S K, LeBlanc S, Goodson K E and Dames C 2013 $ per W metrics for thermoelectric power generation: beyond ZT *Energy Environ. Sci.* **6** 2561–71
[12] Orr B, Akbarzadeh A, Mochizuki M and Singh R 2016 A review of car waste heat recovery systems utilising thermoelectric generators and heat pipes *Appl. Therm. Eng.* **101** 490–5
[13] Dávila D, Tarancón A, Fernández-Regúlez M, Calaza C, Salleras M, San Paulo A and Fonseca L 2011 Silicon nanowire arrays as thermoelectric material for a power microgenerator *J. Micromech. Microeng.* **21** 104007
[14] Fonseca L *et al* 2016 Smart integration of silicon nanowire arrays in all-silicon thermoelectric micro-nanogenerators *Semicond. Sci. Technol.* **31** 084001
[15] Dimaggio E and Pennelli G 2016 Reliable fabrication of metal contacts on silicon nanowire forests *Nano Lett.* **16** 4348–54
[16] Glosch H, Ashauer M, Pfeiffer U and Lang W 1999 A thermoelectric converter for energy supply *Sensors Actuators* A **74** 250
[17] Xie J, Lee C and Feng H 2010 Design, fabrication, and characterization of cmos mems-based thermoelectric power generators *J. Microelectromech. Syst.* **19** 317–24
[18] Ziouche K, Yuan Z, Lejeune P, Lasri T, Leclercq D and Bougrioua Z 2017 Silicon-based monolithic planar micro thermoelectric generator using bonding technology *J. Microelectromech. Syst.* **26** 45–7
[19] Linden D 1984 *Handbook of Batteries and Fuel Cells* (New York: McGraw-Hill)
[20] Olivetti E, Gregory J and Kirchain R 2011 Life cycle impacts of alkaline batteries with a focus on end-of-life *Technical Report* Massachusetts Institute of Technology for NEMA
[21] Ying T-K, Gao X-P, Hu W-K, Wu F and Noreus D 2006 Studies on rechargeable nimh batteries *Int. J. Hydrog. Energy* **31** 530
[22] Mauger A and Julien C M 2017 Critical review on lithium-ion batteries: are they safe? sustainable? *Ionics* **23** 1933–47
[23] Bergveld H J, Kruijt W S, Notten P H L and Notten P H L 2002 Battery management systems: design by modelling *Philips Research Book Series* (Berlin: Springer)
[24] Younesi R, Veith G M, Johansson P, Edström K and Vegge T 2015 Lithium salts for advanced lithium batteries: Li-metal, Li-O_2, and Li-S *Energy Environ. Sci.* **8** 1905–22
[25] Cao C, Li Z-B, Wang X-L, Zhao X-B and Han W-Q 2014 Recent advances in inorganic solid electrolytes for lithium batteries *Front. Energy Res.* **2** 25
[26] Barsukov Y and Qian J 2013 *Battery Power Management for Portable Devices, Norwood, Artech House*
[27] Scrosati B and Vincent C A 2003 *Modern Batteries* (Oxford: Heinemann)
[28] Thermoelectric Generator (TEG) MODULES (II-VI) (https://marlow.com/products/power-generators/thermoelectric-generator-teg-modules).
[29] LeBlanc S, Yee S K, Scullin M L, Dames C and Goodson K E 2014 Material and manufacturing cost considerations for thermoelectrics *Renew. Sustain. Energy Rev.* **32** 327
[30] Yan J, Liao X, Yan D and Chen Y 2018 Review of micro thermoelectric generator *J. Microelectromech. Syst.* **27** 1–18
[31] Snyder G J, Lim J R, Huang C-K and Fleurial J-P 2003 Thermoelectric microdevice fabricated by a MEMS-like electrochemical process *Nat. Mater.* **2** 528
[32] Atthi N, Aramphongphun C, Yanpirat P, Charnsethikul P, Jantawong J, Jeamsaksiri W, Hruanun C and Poyai A 2008 Cost-time analysis for 3D microstructure fabrication using multi-film thickness mask and current techniques *Proc. 3rd World Conf. on Production and Operations Management* pp 1925–40
[33] Kaeslin H 2008 *Digital Integrated Circuit Design: From VLSI Architectures to CMOS Fabrication* (Cambridge: Cambridge University Press)
[34] Cobble M H 1995 Calculations of generator performance *CRC Handbook of Thermoelectrics* ed D M Rowe (Boca Raton, FL: CRC Press) pp 489–501
[35] OECD 2019 Unit labour cost - quarterly indicators - early estimates (Edition 2018) (OECD Publishing) (https://doi.org/10.1787/07d7b75a-en)
[36] Win K K, Dasgupta S and Panda S K 2011 An optimized mppt circuit for thermoelectric energy harvester for low power applications *2011 IEEE 8th Int. Conf. on Power Electronics and ECCE Asia (ICPE and ECCE)* (Piscataway, NJ : IEEE) pp 1579–84
[37] Montecucco A, Siviter J and Knox A R 2014 The effect of temperature mismatch on thermoelectric generators electrically connected in series and parallel *Appl. Energy* **123** 47–54
[38] Bond M and Park J-D 2015 Current-sensorless power estimation and mppt implementation for thermoelectric generators *IEEE Trans. Ind. Electron.* **62** 5539–48
[39] Wu G and Yu X 2012 System design to harvest thermal energy across pavement structure *Proc. 2012 IEEE Energytech (Ohio)* pp 1–4